Object Shape and Reflectance Modeling from Observation

Yoichi Sato[1], Mark D. Wheeler[2], and Katsushi Ikeuchi[1]

[1]Institute of Industrial Science
University of Tokyo

[2]Apple Computer Inc.

ABSTRACT

An object model for computer graphics applications should contain two aspects of information: shape and reflectance properties of the object. A number of techniques have been developed for modeling object shapes by observing real objects. In contrast, attempts to model reflectance properties of real objects have been rather limited. In most cases, modeled reflectance properties are too simple or too complicated to be used for synthesizing realistic images of the object.

In this paper, we propose a new method for modeling object reflectance properties, as well as object shapes, by observing real objects. First, an object surface shape is reconstructed by merging multiple range images of the object. By using the reconstructed object shape and a sequence of color images of the object, parameters of a reflection model are estimated in a robust manner. The key point of the proposed method is that, first, the diffuse and specular reflection components are separated from the color image sequence, and then, reflectance parameters of each reflection component are estimated separately. This approach enables estimation of reflectance properties of real objects whose surfaces show specularity as well as diffusely reflected lights. The recovered object shape and reflectance properties are then used for synthesizing object images with realistic shading effects under arbitrary illumination conditions.

CR Descriptors: I.2.10 [**Artificial Intelligence**]: Vision and Scene Understanding - *Modeling and recovery of physical attributes*; I.3.7 [**Computer Graphics**]: Three-Dimensional Graphics and Realism - *Color, shading, shadowing, and texture*; I.3.3 [**Computer Graphics**]: Picture/Image Generation - *Digitizing and scanning*

1 INTRODUCTION

As a result of significant advancement of graphics hardware and image rendering algorithms, the 3D computer graphics capability has become available even on low-end computers. In addition, the rapid spread of the internet technology has caused a significant increase in the demand for 3D computer graphics. For instance, a new format for 3D computer graphics on the internet, called VRML, is becoming an industrial standard format, and the number of applications using the format is increasing quickly.

However, it is often the case that 3D object models are created manually by users. That input process is normally time-consuming and can be a bottleneck for realistic image synthesis. Therefore, techniques to obtain object model data automatically by observing real objects could have great significance in practical applications.

An object model for computer graphics applications should contain two aspects of information: shape and reflectance properties of the object. A number of techniques have been developed for modeling object shapes by observing real objects. Those techniques use a wide variety of approaches which includes range image merging, shape from motion, shape from shading, and photometric stereo. In contrast, attempts to model reflectance properties of real objects have been rather limited. In most cases, modeled reflectance properties are too simple or too complicated to be used for synthesizing realistic images of the object. For example, if only observed color texture or diffuse texture of a real object surface is used (e.g., texture mapping), correct shading effects such as highlights cannot be reproduced correctly in synthesized images. If highlights on the object surface are observed in original color images, the highlights are treated as diffuse texture on the object surface and, therefore, remain on the object surface permanently regardless of illuminating and viewing conditions. On the other hand, object reflectance properties can be represented accurately by a bidirectional reflectance distribution function (BRDF). If a BRDF is available for the object surface, shading effects can be, in principle, reproduced correctly in synthesized images. However, the use of BRDF is not practical because measurement of BRDF is usually very expensive and time-consuming. In practice, we cannot obtain a BRDF for real objects with various reflectance properties.

Recently, several techniques to obtain object surface shapes and reflectance properties only from intensity images have been developed. Sato and Ikeuchi [15] introduced a method to analyze a sequence of color images taken under a moving light source. They successfully estimated reflectance function parameters, as well as object shape, by explicitly separating the diffuse and specular reflection components. Lu and Little [11] developed a method to estimate a reflectance function from a sequence of black and white images of a rotating smooth object, and the object shape was successfully recovered using the estimated reflectance function. Since the reflectance function is measured directly from the input image sequence, the method does not assume a particular reflection model such as the Lambertian model which is commonly used in computer vision. However, their algorithm can be applied to object surfaces with uniform reflectance properties, and it cannot be easily extended to overcome this limitation.

Another interesting attempt for measuring a reflectance function from intensity images has been reported by Ward [20]. Ward designed a special device with a half-silvered hemisphere and a CCD video camera, which can measure a BRDF of anisotropic reflection.

---

[1] Department of Electrical Engineering and Electronics, Institute of Industrial Science, University of Tokyo, 7-22-1 Roppongi, Minato-ku, Tokyo 106, Japan. {ysato, ki}@iis.u-tokyo.ac.jp. See also http://www.cvl.iis.u-tokyo.ac.jp/~ysato.

[2] Apple Computer Inc., 1 Infinite Loop, MS:301-3M, Cupertino, CA 95014. mdwheel@apple.com.

The main advantage of the device is that it takes significantly less time to measure a BRDF than a conventional gonioreflectometer. A BRDF of a real object surface has been measured by the device and highly realistic images have been synthesized. However, this approach cannot be easily extended for modeling real objects with various reflectance properties. This approach still requires a small piece of test material for measuring the material's BRDF.

Techniques to measure object surface shape and reflectance properties simultaneously by using both range images and black and white intensity images have been studied by other researchers. Ikeuchi and Sato [7] originally developed a method to measure object shapes and reflection function parameters from a range image and intensity image pair. In their attempt, the surface shape is recovered from the range image at first, and then surface normals of the recovered object surface are used for reflectance parameter estimation. The main drawback of the method is that it assumes uniform reflectance properties over the object surface. Additionally, only partial object shape was recovered because only one range image was used.

Baribeau, Rioux, and Godin [1] measured three reflectance parameters that they call the diffuse reflectance of the body material, the Fresnel reflectance of the air-media interface, and the slope surface roughness of the interface, by using their polychromatic laser range sensor which can produce a pair of range and color images. Their method could estimate more detailed reflectance properties than the one developed by Ikeuchi and Sato [7]. However, their method still required uniform reflectance properties over each object surface, and only partial object shape was recovered.

Kay and Caelli [9] introduced another method to use a range image and 4 or 8 intensity images taken under different illumination conditions. By increasing the number of intensity images, they estimated reflection function parameters locally for each image pixel. Unlike the algorithm proposed by Sato and Ikeuchi, the method can handle object surfaces with varying reflectance properties. However, it is reported that parameter estimation can be unstable, especially when the specular reflection component is not observed strongly.

More recently, Sato and Ikeuchi developed a method to measure object surface shape and reflectance properties from a sequence of range and color images [16]. The method has an advantage over other methods in that it can handle objects with non-uniform reflectance properties. However, the method relies on region segmentation on object surfaces, and each of the segmented regions must have uniform reflectance properties. Therefore, the method cannot be applied to highly textured objects.

In this paper, we propose a new method for modeling object reflectance properties, as well as object shapes, from multiple range and color images of real objects. Unlike previously proposed methods, our method can create complete object models, i.e., not partial object shape, with non-uniform reflectance properties. First, the object surface shape is reconstructed by merging multiple range images of the object. By using the reconstructed object shape and a sequence of color images of the object, parameters of a reflection model are estimated in a robust manner. The key point of the proposed method is that, first, the diffuse reflection components and the specular reflection component are separated from the color image sequence, and then, reflectance parameters of each reflection component are estimated separately. Unlike previously reported methods, this approach enables reliable estimation of surface reflectance properties which are not uniform over the object surface, and which include specularity as well as diffusely reflected lights. We demonstrate the capability of our object modeling technique by synthesizing object images with realistic shading effects under arbitrary illumination conditions.

This paper is organized as follows: Section 2 describes our image acquisition system for obtaining a sequence of range and color images of the object. Section 3 explains reconstruction of the object surface shape from the range image sequence. Section 4 describes our method for estimating reflectance properties of the object using the reconstructed object shape and the color image sequence. Object images synthesized using the recovered object shape and reflectance properties are shown in Section 5. Concluding remarks are presented in Section 6.

2 IMAGE ACQUISITION SYSTEM

The experimental setup for the image acquisition system used in our experiments is illustrated in Figure 1. The object whose shape and reflectance information is to be recovered is mounted on the end of a robotic arm. The object used in our experiment is a ceramic mug whose height is about $100mm$. Using the system, a sequence of range and color images of the object is obtained as the object is rotated at a fixed angle step. Twelve range images and 120 color images were used in our experiment shown in this paper.

A range image is obtained using a light-stripe range finder with a liquid crystal shutter and a color CCD video camera [14]. 3D locations of points in the scene are computed at each image pixel using optical triangulation. Each range-image pixel represents an (X, Y, Z) location of a corresponding point on an object surface. The same color camera is used for acquiring range images and color images. Therefore, pixels of the range images and the color images directly correspond.

The range finder is calibrated to produce a 3×4 projection matrix Π which represents the projection transformation between the world coordinate system and the image coordinate system. The location of the PUMA 560 manipulator with respect to the world coordinate system is also found via calibration. Therefore, the object location is given as a 4×4 transformation matrix T for each digitized image.

A single incandescent lamp is used as a point light source. In our experiments, the light source direction and the light source color are measured by calibration. The gain and offset of outputs from the video camera are adjusted so that the light source color becomes $(R, G, B) = (1, 1, 1)$.

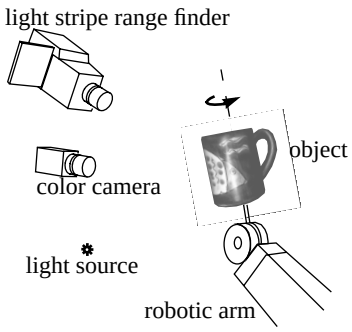

Figure 1 *Image acquisition system*

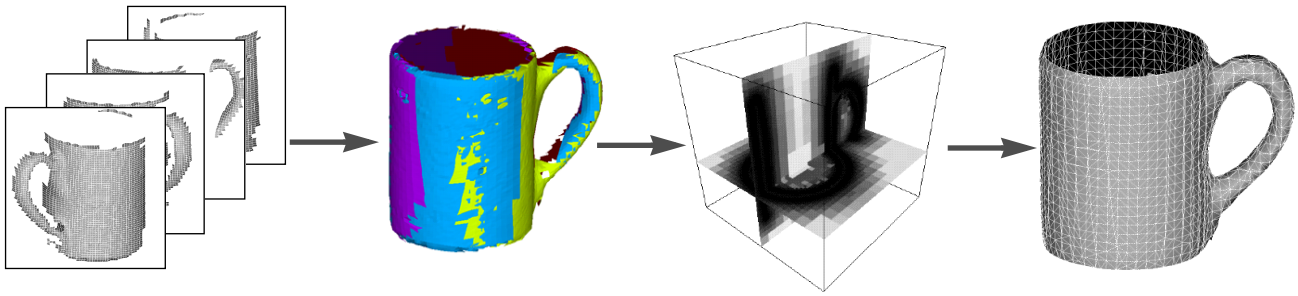

(a) range image acquisition (b) alignment (c) merging (d) isosurface extraction

Figure 2 *Shape reconstruction by merging range images: (a) Input surface patches (4 out of 12 patches are shown), (b) Result of alignment, (c) Obtained volumetric data (two cross sections are shown), (d) Generated triangular mesh of the object shape (3782 triangles)*

3 SURFACE SHAPE MODELING

A sequence of range images of the object is used to construct the object shape as a triangular mesh. Then, the number of triangles used for the object shape model is reduced by simplifying the object shape without losing its details for efficient storage and rendering of the object.

One disadvantage of using the simplified object model is that a polygonal normal computed from the simplified triangular mesh model does not accurately approximate the real surface normal even though the object shape is preserved reasonably well. Thus, rather than using polygonal normals, we compute surface normals at dense grid points within each triangle of the object surface mesh by using the lowest level input, i.e., 3D points measured in range images.

In Section 3.1, we describe reconstruction of a triangular mesh model of the object from a sequence of range images. Estimation of dense surface normals is explained in Section 3.2.

3.1 Shape modeling from range image merging

For reconstructing object shapes as a triangular mesh model from multiple range images, we used the volumetric method developed by Wheeler, Sato, and Ikeuchi [21]. The method consists of the following four steps, each of which is briefly described in this section.

1. Surface acquisition from each range image

The range finder in our image acquisition system cannot measure the object surface itself. In other words, the range finder can produce only images of 3D points on the object surface. Because of this limitation, we need to somehow convert the measured 3D points into a triangular mesh which represents the object surface shape. This is done by connecting two neighboring range image pixels based on the assumption that those points are connected by a locally smooth surface. If those two points are closer in a 3D distance than some threshold, then we consider them to be connected on the object surface.

In Figure 2 (a), 4 out of 12 input range images of the mug are shown as triangular meshes.

2. Alignment of all range images

All of the range images are measured in the coordinate system fixed with respect to the range finder system, and they are not aligned to each other initially. Therefore, after we obtain the triangular surface meshes from the range images, we need to transform all of the meshes into a unique object coordinate system.

To align the range images, we use a transformation matrix T which represents the object location for each range image (Section 2). Suppose we select one of the range images as a key range image to which all other range images are aligned. We refer to the transformation matrix for the key range image as T_{merge}. Then, all other range images can be transformed into the key range image's coordinate system by transforming all 3D points $P = (X, Y, Z, 1)$ as $P' = T_{merge} T_f^{-1} P$ where $f = 1 \ldots n$ is a range image frame number.

3. Merging based on a volumetric representation

After all of the range images are converted into triangular patches and aligned to a unique coordinate system, we merge them using a volumetric representation. First, we consider imaginary 3D volume grids around the aligned triangular patches. Then, in each voxel,[3] we store the value, $f(x)$, of the signed distance from the center point of the voxel, x, to the closest point on the object surface. The sign indicates whether the point is outside, $f(x) > 0$, or inside, $f(x) < 0$, the object surface, while $f(x) = 0$ indicates that x lies on the surface of the object.

This technique has been applied to surface extraction by several researchers [5], [3], [4]. The novel part of our technique is the robust computation of the signed distance. Our technique computes the signed distance by using a new algorithm called *the consensus surface algorithm* [21]. In the consensus surface algorithm, a quorum of consensus of locally coherent observation of the object surface is used to compute the signed distance correctly, which eliminates many of the troublesome effects of noise and extraneous surface observations in the input range images, for which previously developed methods are susceptible.

One drawback of using a volume grid for merging range images is the amount of memory required for the volume grid, which is $O(n^3)$ and therefore quickly becomes prohibitively large as the resolution n increases. Curless and Levoy's method [3] used

3. **voxel:** volume element

a run-length encoding to overcome this problem. In our technique, an oct-tree structure [8] is used, and the required memory was reduced to $4 - 23$ % for several examples reported in [21]. Further study is needed to determine whether the use of oct-trees as in our technique is more or less efficient than the run-length encoding in Curless and Levoy's method.

Figure 2 (c) shows two cross sections of the volumetric data constructed from the input range images of the mug. A darker color represents a shorter distance to the object surface, and a brighter color represents a longer distance.

4. Isosurface extraction from volumetric grid

The volumetric data is then used to construct the object surface as a triangular mesh. The marching cubes algorithm [10] constructs a triangular mesh by traversing zero crossings of the implicit surface, $f(x) = 0$, in the volume grid. Here, the marching cube algorithm was modified so that it handles holes and missing data correctly [21].

Figure 2 (d) shows the result of triangular mesh reconstruction. In this example, 3782 triangles were generated from the volumetric data.

The marching cube algorithm generally produces a large number of triangles whose sizes vary significantly. Thus, it is desirable to simplify the reconstructed object surface shape by reducing the number of triangles. We used the mesh simplification method developed by Hoppe et al. [6] for this purpose. In our experiment, the total number of triangles was reduced from 3782 to 488 (Figure 3).

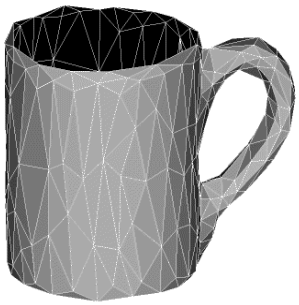

Figure 3 Simplified shape model: The object shape model was simplified from 3782 to 488 triangles.

3.2 Surface normal estimation

Polygonal normals computed from a triangular surface mesh model can approximate real surface normals fairly well when the object surface is relatively smooth and does not have high curvature points. However, accuracy of polygonal normals becomes poor when the object surface has high curvature points and the resolution of the triangular surface mesh model is low, i.e., a smaller number of triangles to represent the object shape.

This becomes a problem especially for the task of reflectance parameter estimation. For estimating reflectance parameters at a surface point, we need to know three directions at the surface point: the viewing direction, the light source direction, and the surface normal. As a result, with incorrectly estimated surface normals, small highlights observed within each triangle cannot be analyzed accurately, and therefore they cannot be reproduced in synthesized images. For this reason, we compute surface normals at regular grid points (20×20 points in our experiment) within each triangle using the 3D points from the range images. The resolution of regular grid points should be changed depending on the size of each triangle, so that the density of grid points becomes more or less uniform over the object surface. The adaptive resolution of grid points is yet to be implemented in our object modeling system.

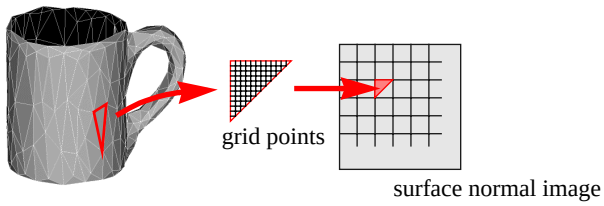

Figure 4 Dense surface normal estimation

The surface normal at a grid point P_g is determined from a least squares best fitting plane to all neighboring 3D points whose distances to the point P_g are shorter than some threshold. This surface normal estimation method has been used by other researchers for other applications. Cromwell [2] used a similar method for choosing the best direction for viewing a cloud of small particles, e.g., molecules, in computer graphics. Hoppe et al. [5] used the surface normal estimation method for surface reconstruction from a cloud of 3D points.

The surface normal is computed as an eigen vector of the covariance matrix of the neighboring 3D points; specifically, the eigen vector associated with the eigenvalue of smallest magnitude (Figure 5). The covariance matrix of n 3D points $[X_i, Y_i, Z_i]^T$, with centroid $[\bar{X}, \bar{Y}, \bar{Z}]^T$, is defined as

$$C = \sum_{i=1}^{n} \begin{bmatrix} (X_i - \bar{X}) \\ (Y_i - \bar{Y}) \\ (Z_i - \bar{Z}) \end{bmatrix} \begin{bmatrix} (X_i - \bar{X}) & (Y_i - \bar{Y}) & (Z_i - \bar{Z}) \end{bmatrix}. \qquad (1)$$

The surface normals computed at regular grid points within each triangle are then stored as a three-band surface normal image which is later used for mapping dense surface normals to the triangular mesh of the object shape. The mapped surface normals are used both for reflectance parameter estimation and for rendering color images of the object.

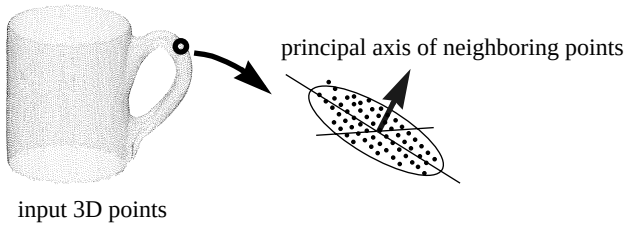

Figure 5 *Surface normal estimation from input 3D points*

4 SURFACE REFLECTANCE MODELING

After the object shape is reconstructed, we measure reflectance properties of the object surface using the reconstructed shape and the input color images. First, the two fundamental reflection components (i.e., the diffuse and specular reflection components)

are separated from the input color images. Then, the parameters for the two reflection components are estimated separately. Separation of the two reflection components enables us to obtain a reliable estimation of the specular reflection parameters. Also, the specular reflection component (i.e., highlight) in the color images does not affect estimated diffuse reflection parameters of the object surface.

In Section 4.1 we introduce the reflection model used in this analysis. Then, in Section 4.2 we describe how to determine an observed color sequence for a 3D point on the object surface from the input color images. Using the observed color sequence, the algorithm for separating the diffuse and specular reflection components is explained in Section 4.3. We explain the measurement of the diffuse reflection parameters in Section 4.4. Finally, we describe the estimation of the specular reflection parameters in Section 4.5.

4.1 Reflection model

A general reflection model is described in terms of three reflection components, namely the diffuse lobe, the specular lobe, and the specular spike [12]. In many computer vision and computer graphics applications, reflection models are represented by linear combinations of two of those reflection components: the diffuse lobe component and the specular lobe component. The specular spike component can be observed only from mirror-like smooth surfaces where reflected light rays of the specular spike component are concentrated in a specular direction. It is thus difficult to observe the specular spike component from a coarsely sampled set of viewing directions.

The diffuse lobe component and the specular lobe component are normally called the diffuse reflection component and the specular reflection component, respectively. This reflection model was formally introduced by Shafer as the dichromatic reflection model [17].

In our analysis, the Torrance-Sparrow model [19] is used for representing the diffuse and specular reflection components. As Figure 1 illustrates, the illumination and viewing directions are fixed with respect to the world coordinate system. The reflection model used in our analysis is given as

$$I_m = K_{D,m}\cos\theta_i + K_{S,m}\frac{1}{\cos\theta_r}e^{-\alpha^2/2\sigma^2} \quad m = R, G, B \tag{2}$$

where θ_i is the angle between the surface normal and the light source direction, θ_r is the angle between the surface normal and the viewing direction, α is the angle between the surface normal and the bisector of the light source direction and the viewing direction, $K_{D,m}$ and $K_{S,m}$ are constants for the diffuse and specular reflection components, and σ is the standard deviation of a facet slope of the Torrance-Sparrow model.

This reflection model represents reflections which bounce only once from the light source. Therefore, the reflection model is valid only for convex objects, and it cannot represent interreflections on concave object surfaces. However, we empirically determined that interreflection did not affect our analysis significantly.

In this paper, we refer to $K_{D,R}$, $K_{D,G}$, and $K_{D,B}$ as the diffuse reflection parameters, and $K_{S,R}$, $K_{S,G}$, $K_{S,B}$, and σ as the specular reflection parameters.

4.2 Mapping color images onto object surface shape

For separating the diffuse and specular reflection components and for estimating parameters of each reflection component, we need to know a sequence of observed colors at each point on the object surface as the object is rotated. In this section, we describe how to obtain an observed color sequence of a surface point (X,Y,Z) from the input color image sequence.

We represent world coordinates and image coordinates using homogeneous coordinates. A point on the object surface with Euclidean coordinates (X, Y, Z) is expressed by a column vector $P = [X, Y, Z, 1]^T$. An image pixel location (x, y) is represented by $p = [x, y, 1]^T$. As described in Section 2, the camera projection transformation is represented by a 3×4 matrix Π, and the object location is given by a 4×4 object transformation matrix T. We denote the object transformation matrix for the input color image frame f by T_f $(f = 1 \ldots n)$. Thus, using the projection matrix Π and the transformation matrix T_{merge} for the key range image (Section 3.1), the projection of a 3D point on the object surface in the color image frame f is given as

$$p_f = \Pi T_f T_{merge}^{-1} P \qquad (f = 1 \ldots n) \tag{3}$$

where the last component of p_f has to be normalized to give the projected image location (x, y).

The observed color of the 3D point in the color image frame f is given as the (R, G, B) color intensity at the pixel location (x, y). If the 3D point is not visible in the color image (i.e., the point is facing away from the camera, or it is occluded), the observed color for the 3D point is set to $(R, G, B) = (0, 0, 0)$. By repeating this procedure for all frames of the input color image sequence, we get an observed color sequence for the 3D point on the object surface.

Figure 6 shows the result of mapping the input color images onto the reconstructed object surface shape.

4.3 Reflection component separation from color image sequence

We now describe the algorithm for separating the two reflection components. This separation algorithm was originally introduced for the case of a moving light source by Sato and Ikeuchi [15]. In this paper, a similar algorithm is applied for the case of a moving object.

Using three color bands, red, green, and blue, the coefficients $K_{D,m}$ and $K_{S,m}$, in Equation (2), generalize to two linearly independent vectors,

$$\underset{\sim}{K}_D = \left[K_{D,R}\ K_{D,G}\ K_{D,B}\right]^T \quad \underset{\sim}{K}_S = \left[K_{S,R}\ K_{S,G}\ K_{S,B}\right]^T \tag{4}$$

unless the colors of the two reflection components are accidentally the same.

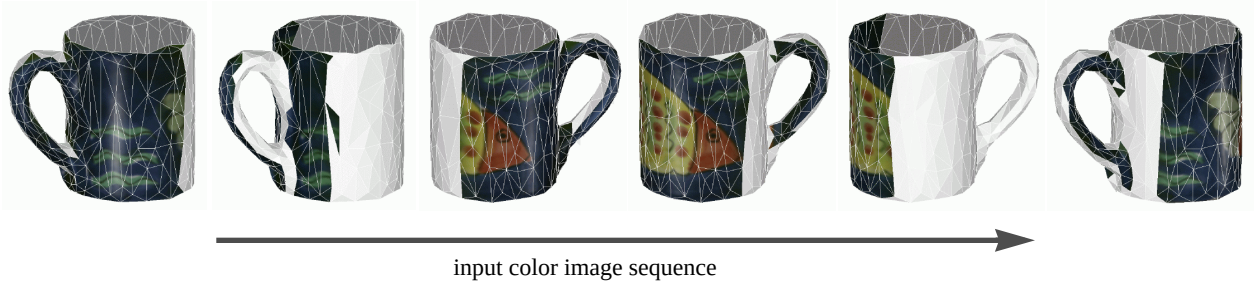

Figure 6 *Color image mapping result: 6 out of 120 color images are shown here.*

First, the color intensities in the R, G, and B channels from input images of the object are measured for each point on the object surface as described in Section 4.2. The three sequences of intensity values are stored in the columns of an $n \times 3$ matrix M. Considering the reflectance model (Equation (2)) and two color vectors in Equation (4), the intensity values in the R, G, and B channels can be represented as

$$\begin{aligned} M &= \left[\underset{\sim}{M}_R \; \underset{\sim}{M}_G \; \underset{\sim}{M}_B\right] \\ &= \begin{bmatrix} \cos\theta_{i1}\, E(\theta_{r1}, \alpha_1) \\ \cos\theta_{i2}\, E(\theta_{r2}, \alpha_2) \\ \vdots \\ \cos\theta_{in}\, E(\theta_{rn}, \alpha_n) \end{bmatrix} \begin{bmatrix} K_{D,R} & K_{D,G} & K_{D,B} \\ K_{S,R} & K_{S,G} & K_{S,B} \end{bmatrix} \\ &= \left[\underset{\sim}{G}_D \; \underset{\sim}{G}_S\right] \begin{bmatrix} \underset{\sim}{K}_D^T \\ \underset{\sim}{K}_S^T \end{bmatrix} \\ &\equiv GK \end{aligned} \tag{5}$$

where $E(\theta_r, \alpha) = exp(-\alpha^2/2\sigma^2)/\cos\theta_r$, and the two vectors $\underset{\sim}{G}_D$ and $\underset{\sim}{G}_S$ represent the intensity values of the diffuse and specular reflection components with respect to the illuminating/viewing directions θ_i, θ_r, and α. The vectors $\underset{\sim}{K}_D$ and $\underset{\sim}{K}_S$ represent the diffuse and the specular reflection color vectors, respectively.

Suppose we have an estimate of the matrix K. Then, the two reflection components represented by the matrix G are obtained by projecting the observed reflection stored in M onto the two color vectors $\underset{\sim}{K}_D$ and $\underset{\sim}{K}_S$ as

$$G = MK^+ \tag{6}$$

where K^+ is the 3×2 pseudoinverse matrix of the color matrix K.

The derivation shown above is based on the assumption that the matrix K is known. In our experiments, the specular reflection color vector $\underset{\sim}{K}_S$ is directly measured as the light source color by a calibration procedure. Therefore, only the diffuse color vector $\underset{\sim}{K}_D$ is unknown and needs to be determined.

From Equation (2), it can be seen that the distribution of the specular reflection component is limited to a fixed angle, depending on σ. Thus, if the angle α is sufficiently large at a point on the object surface, an observed color at the point should represent the color of the diffuse reflection component. The angles α, θ_i, and θ_r are computed using the object transformation matrix T_f ($f = 1 \ldots n$) and the camera projection matrix Π as follows. The light source location is acquired via calibration, and the camera projection center can be computed from the projection matrix Π. Also, the surface normal at the surface point of the object model for the color image frame f can be computed by rotating the surface normal at the surface point by the object transformation matrix T_f. Using the light source direction, the viewing direction and the surface normal, α, θ_i, and θ_r are computed.

Once we get the matrix K, the matrix G can be calculated from Equation (6). Each of the diffuse and specular reflection components is given as

$$M_D = \underset{\sim}{G}_D \underset{\sim}{K}_D^T \qquad M_S = \underset{\sim}{G}_S \underset{\sim}{K}_S^T . \tag{7}$$

Figure 7 (a) illustrates a typical observed color sequence with specularity. The separation algorithm was applied to the observed color sequence, and the separation result is shown in Figure 7 (b).

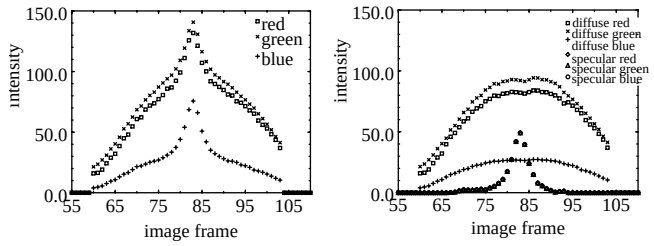

Figure 7 *(a) observed color sequence and (b) separation result*

Another technique for separating the diffuse and specular reflection components is the use of polarization filters [13] [22]. The technique could be used for separating reflection components instead of the one described in this section. However, the use of polarization generally requires more samplings of images by using a more complex image acquisition system. Thus, we have not explored this direction in our study.

4.4 Diffuse reflection parameter estimation

Using the diffuse reflection component separated from the observed color sequence, we now can estimate the diffuse reflec-

tion parameters ($K_{D,R}$, $K_{D,G}$, and $K_{D,B}$) without undesirable effects from the specular reflection component (i.e., highlights). Using the angle θ_i computed as stated in the previous section, the diffuse reflection parameters are estimated by fitting the reflection model (the first term of Equation (2)) to the separated diffuse reflection component. Hence, the estimated diffuse reflection parameters are not affected by the particular shadings in the observed images, e.g., the effect of the light source can be factored out. In other words, the diffuse reflection parameters can be estimated correctly even if the object appears dark or bright in the color images.

The diffuse reflection parameters are estimated at regular grid points within each triangle just as the surface normals in Section 3.2 are estimated. The resolution of the grid of points is 80×80 in our experiment, while it is 20×20 for the surface normal estimation. The higher resolution is necessary to capture details of the diffuse reflection texture on the object surface. The resolution for the diffuse reflection parameter estimation should be determined by the average number of pixels which fall onto one triangle of the object shape model in the observed color images. Resolution higher than the average number does not capture any more information than that in the observed color images, but it increases the required storage for the diffuse reflection parameters unnecessarily. Figure 8 shows the result of the diffuse reflection parameter estimation where the estimated parameters are visualized as surface texture on the mug.

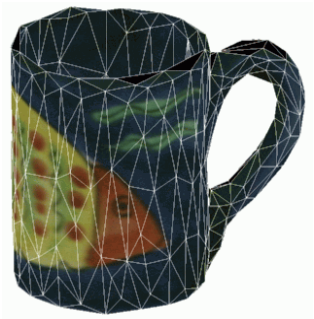

Figure 8 Estimated diffuse reflection parameters

4.5 Specular reflection parameter estimation

As in the diffuse reflection parameter estimation, the specular reflection parameters ($K_{S,R}$, $K_{S,G}$, $K_{S,B}$, and σ) are also computed using the angle θ_r and the angle α. However, there is a significant difference between estimation of the diffuse and specular reflection parameters. The diffuse reflection parameters can be estimated as long as the object surface is illuminated and viewed from the camera. On the other hand, the specular reflection component is usually observed only from a limited range of viewing directions. For a finite set of views, the specular reflection component will only be observed over a small portion of the object surface in the input color image sequence. For much of the object surface, we cannot estimate the specular reflection parameters. Even if the specular reflection component is observed, the parameter estimation can become unreliable if the specular reflection component is not observed strongly, or if the separation of the two reflection components is not performed well.

For the above reasons, we decided to use a slightly different strategy for estimating the specular reflection parameters. Since the specular reflection parameters may only be estimated sparsely over the object surface, we use interpolation to infer the specular reflection parameters over the entire surface.

In Section 4.5.1, we describe how to select object surface points which are suitable for estimating the specular reflection parameters. Interpolation of the estimated specular reflection parameters on the object surface is explained in Section 4.5.2.

4.5.1 Selection of Surface Points for Parameter Estimation

For the specular refection parameters to be estimated reliably, the following three conditions are necessary at a point on the object surface. All of the three conditions contribute to reliable separation of the diffuse and specular reflection components.

1. The two reflection components must be reliably separated. Because the diffuse and specular reflection components are separated using the difference of the colors of the two components (Section 4.3), these color vectors should differ as much as possible. This can be examined by saturation of the diffuse color (Figure 9). Since the light source color is generally close to white (saturation = 0), if the diffuse color has a high saturation value, the diffuse and specular reflection colors will be different.

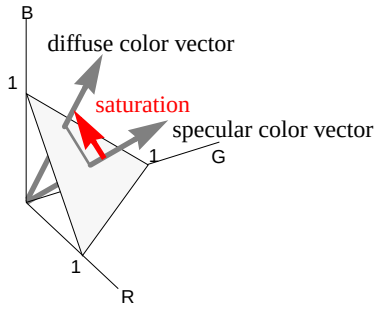

Figure 9 Diffuse saturation shown in the RGB color space

2. The magnitude of the specular reflection component is as large as possible.

3. The magnitude of the diffuse reflection component is as large as possible. Although this condition might seem to be unnecessary, we empirically found that the specular reflection parameters can be obtained more reliably if this condition is satisfied.

Figure 10 Selected vertices for specular parameter estimation: 100 out of 266 vertices were selected.

An evaluation measure: *v = diffuse saturation * max specular intensity * max diffuse intensity* is used to represent how well these three conditions are satisfied. In our experiments, we used the vertices of the triangular surface mesh as candidates for parameter estimation. Then, *100* vertices with the largest values were chosen according to our evaluation measurement v. Figure 10 illustrates 100 selected vertices for specular parameter estimation out of 266

vertices. Note that the use of the triangular vertices as initial candidates for specular parameter estimation is not essential in our method. In practice, we found that this choice was sufficient to find suitable points for specular parameter estimation.

4.5.2 Interpolation of Estimated Specular Parameters

In our experiment, the camera output is calibrated so that the specular reflection color (i.e., the light source color) has the same value from the three color channels (Section 2). For instance, the separated specular reflection component shown in Figure 7 (b) has more or less the same output from the three color channels. Therefore, only one color band was used to estimate the specular reflection parameters (K_S and σ) in our experiment.

After the specular reflection parameters K_S and σ were estimated at the 100 selected vertices, the estimated values were linearly interpolated based on a distance on the object surface, so that the specular reflection parameters were obtained at regular grid points within each triangle of the object surface mesh. The resolution of the grid points was 20×20 in our experiment, while the resolution was 80×80 for the diffuse reflection parameter estimation. In general, specular reflectance does not change so rapidly as diffuse reflectance, i.e., diffuse texture on the object surface. Therefore, the resolution of 20×20 was enough to capture the specular reflectance of the mug.

Interpolated values of the two specular reflection parameters are shown in Figure 11. The obtained specular reflection parameters were then stored in two specular reflection parameter images (a K_S image and a σ image) just as estimated surface normals were stored in the surface normal image.

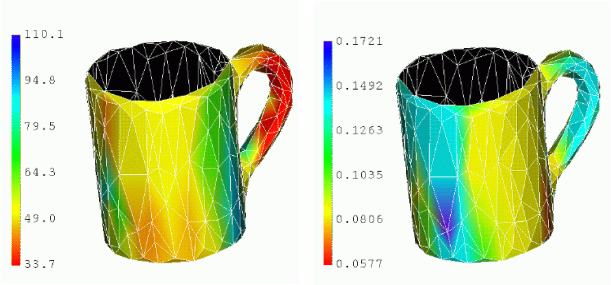

Figure 11 Interpolated K_S and σ

5 IMAGE SYNTHESIS

Using the reconstructed object shape (Section 3.1), the surface normal image (Section 3.2), the diffuse reflection parameter image (Section 4.4), the specular reflection parameter image (Section 4.5), and the reflection model (Equation (2)), we can synthesize color object images under arbitrary illumination/viewing conditions.

Figure 12 shows synthesized images of the object with two point light sources. Note that the images represent highlights on the object surface naturally. For comparing synthesized images with the input color images of the object, the object model was rendered using the same illumination and viewing directions as some of the input color images. Figure 13 shows two frames of the input color image sequence as well as two synthesized images that were generated using the same illuminating/viewing condition as the input color images. It can be seen that the synthesized images closely resemble the corresponding real images. In particular, highlights, which generally are a very important cue of surface material, appear on the side and the handle of the mug naturally in the synthesized images.

However, we can see that the synthesized images are slightly more blurred than the original color images, e.g., the eye of the painted fish in frame 50. That comes from slight error in the measured object transformation matrix T (Section 2) due to imperfect calibration of the robotic arm. Because of the error in the measured transformation matrix T, the projected input color images (Section 4.2) were not perfectly aligned on the reconstructed object surface. As a result, the estimated diffuse reflection parameters were slightly blurred. This blurring effect can be avoided if, after a color image is projected onto the object surface, the color image is aligned with previously projected images by a local search on the surface. However, we have not yet tested this idea in our implementation.

6 CONCLUSION

We have explored automatic generation of photorealistic object models from observation. Achieving photorealism in synthesized object images requires accurate modeling of shape and reflectance properties of the object. In this paper, we have presented a new paradigm for acquiring object shape and reflectance parameters from range and color images.

The object surface shape is reconstructed by merging multiple range images of the object. By using the reconstructed object shape and multiple color images of the object, parameters of the Torrance-Sparrow reflection model are estimated. For estimating reflectance parameters of the object robustly, our method is based on separation of the diffuse and specular reflection components from a color image sequence. Using separated reflection components, reflection model parameters for each of the two components were estimated separately. In particular, the specular reflection parameters were successfully obtained by identifying suitable surface points for estimation and by interpolating estimated parameters over the object surface.

Our experiments have shown that our object modeling method can be effectively used for synthesizing realistic object images under arbitrary illumination and viewing conditions.

Acknowledgment: The authors thank Marie Elm for her valuable comments of the draft of the paper.

REFERENCES

[1] R. Baribeau, M. Rioux, and G. Godin, “Color reflectance modeling using a polychromatic laser sensor,” *IEEE Trans. on Pattern Analysis and Machine Intelligence*, vol. 14, no. 2, pp. 263-269, 1992.

[2] R. L. Cromwell, “Efficient eigenvalues for visualization,” in P. S. Heckbert, editor, *Graphics Gems IV,* Academic Press, San Diego, 1994.

[3] B. Curless and M. Levoy, “A volumetric method for building complex models from range images,” *Computer Graphics (SIGGRAPH ‘96 Proceedings)*, pp. 303-312, 1996.

[4] A. Hilton, J. Stoddart, J. Illingworth, and T. Windeatt, “Reliable surface reconstruction from multiple range images,” *Proceedings of European Conference on Computer Vision ‘96*, pp. 117-126, 1996.

[5] H. Hoppe, T. DeRose, T. Duchamp, J. McDonald, and W. Stuetzle,

"Surface reconstruction from unorganized points," *Computer Graphics (SIGGRAPH '92 Proceedings)*, pp. 71-78, 1992.

[6] H. Hoppe, T. DeRose, T. Duchamp, J. McDonald, and W. Stuetzle, "Mesh Optimization," *Computer Graphics (SIGGRAPH '93 Proceedings)*, pp. 19-26, 1993.

[7] K. Ikeuchi and K. Sato, "Determining reflectance properties of an object using range and brightness images," *IEEE Trans. on Pattern Analysis and Machine Intelligence*, vol. 13, no. 11, pp. 1139-1153, 1991.

[8] C. L. Jackins and S. L. Tanimoto, "Oct-trees and their use in representing three-dimensional objects," *Computer Graphics Image Processing*, vol. 14, no. 3, pp. 249-270, 1980.

[9] G. Kay and T. Caelli, "Inverting an illumination model from range and intensity maps," *CVGIP: Image Understanding*, vol. 59, pp. 183-201, 1994.

[10] W. E. Lorensen and H. E. Cline, "Marching cubes: a high resolution 3D surface construction algorithm," *Computer Graphics (SIGGRAPH '87 Proceedings)*, vol. 21, no. 4, pp. 163-169, 1987.

[11] J. Lu and J. Little, "Reflectance function estimation and shape recovery from image sequence of a rotating object," *Proceedings of International Conference on Computer Vision*, pp. 80-86, June 1995.

[12] S. K. Nayar, K. Ikeuchi, and T. Kanade, "Surface reflection: physical and geometrical perspectives," *IEEE Trans. on Pattern Analysis and Machine Intelligence*, vol. 13, no. 7, pp. 611-634, 1991.

[13] S. K. Nayar, X. Fang, and T. E. Boult, "Removal of specularities using color and polarization," *Proceedings of Computer Vision and Pattern Recognition '93*, pp. 583-590, New York City, NY, June 1993.

[14] K. Sato, H. Yamamoto, and S. Inokuchi, "Range imaging system utilizing nematic liquid crystal mask," *Proceedings of International Conference on Computer Vision*, pp. 657-661, 1987.

[15] Y. Sato and K. Ikeuchi, "Temporal-color space analysis of reflection," *Journal of Optical Society of America A*, vol. 11, no. 11, pp. 2990-3002, November 1994.

[16] Y. Sato and K. Ikeuchi, "Reflectance analysis for 3D computer graphics model generation," *Graphical Models and Image Processing*, vol. 58, no. 5, pp. 437-451, September 1996.

[17] S. Shafer, "Using color to separate reflection components," *COLOR Research and Application*, vol. 10, no. 4, pp. 210-218, 1985.

[18] R. Szelski at Micro Soft Co., *personal communication*.

[19] K. E. Torrance and E. M. Sparrow, "Theory for off-specular reflection from roughened surface," *Journal of Optical Society of America*, vol. 57, pp. 1105-1114, 1967.

[20] G. J. Ward, "Measuring and modeling anisotropic reflection," *Computer Graphics (SIGGRAPH 92Proceedings)*, vol. 26, no. 2, pp. 265-272, 1992.

[21] M. D. Wheeler, Y. Sato, and K. Ikeuchi, "Consensus surfaces for modeling 3D objects from multiple range images," *DARPA Image Understanding Workshop*, 1997.

[22] L. B. Wolff, T. E. Boult, "Constraining object features using a polarization reflectance model," *IEEE Trans. on Pattern Analysis and Machine Intelligence*, vol. 13, no. 6, pp. 635-657, 1991.

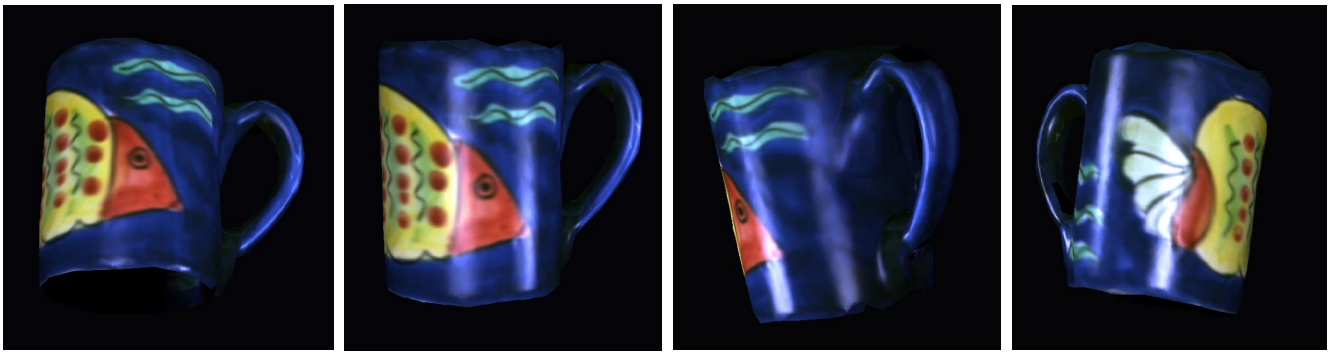

Figure 12 *Synthesized object images*

input frame 50 **synthesized** **input** frame 80 **synthesized**

Figure 13 *Comparison of input color images and synthesized images*